Physics Letters A 380 (2016) 1964–1970

Contents lists available at ScienceDirect

Physics Letters A

www.elsevier.com/locate/pla

Noise-sustained synchronization of electrically coupled FitzHugh–Nagumo networks under counterphase external forcing

Alejandro D. Sánchez [1], Gonzalo G. Izús [*,1]

IFIMAR (Universidad Nacional de Mar del Plata and CONICET), Deán Funes 3350, B7602AYL Mar del Plata, Argentina

ARTICLE INFO

Article history:
Received 11 December 2015
Received in revised form 8 April 2016
Accepted 9 April 2016
Available online 14 April 2016
Communicated by C.R. Doering

Keywords:
Synchronization
Coupled cells
Neural networks

ABSTRACT

We study the stochastic dynamics of two electrically coupled networks of excitable FitzHugh–Nagumo cells, each of them phase-repulsively linked to form a ring able to develop noise-sustained structures. All cells are submitted to Gaussian white noises with common intensity η, while each network is forced with opposite phase by an adiabatic subthreshold harmonic signal. In terms of the nonequilibrium potential of a four-cell reduced model we have interpreted the dynamics, explained the observed activation and synchronization of the structures, and calculated the optimal η level as a function of coupling strength between networks. The values obtained from the reduced model coincide in order of magnitude with those arising from numerical simulations of the full system.

1. Introduction

The constructive effects of noise on the dynamics of complex systems [1–3] is a field of ever increasing interest and activity during the last decades which has uncovered phenomena like stochastic resonance [4–7], coherent resonance [8], and noise-sustained synchronization [9,10] in non-linear dynamical systems. These phenomena are of particular relevance in understanding key issues in neuroscience, where single neurons are often described as relaxation oscillators [11] displaying excitable behavior. In this sense, it is well known that synchronization is relevant for the efficient processing and transmission of information in neural networks (see e.g. [12,13]) and experiments have shown that synchronized states can occur in many special areas of the brain, such as the olfactory system or the hippocampal region [14–16]. The insight gained through detailed theoretical studies of neuron synchronization in networks [17–23] has wide applicability in neuroscience. Examples are the synchronization of gap-junction coupled neurons [21], as well as phase locking and synchronization in neural networks (studied by means of the phase resetting curve) [24,25]. Moreover, noise-induced and noise-enhanced synchronization have also been reported in neuronal systems [26,27].

In realistic neural networks, excitatory and inhibitory synapses are known coexist [28–30]. Previous research has shown that both phase-attractive and phase-repulsive coupling exist in systems of realistic neurons, associated respectively to excitatory and inhibitory synapses. Effects of phase-repulsive coupling on neuronal dynamics have been investigated in [31–33]. For example, it has been shown that a pair of excitable FitzHugh–Nagumo (FHN) neurons can exhibit various firing patterns (including multistability and chaotic firing) when elements interact phase-repulsively [31]. Antiphase coupling plays an important role in circadian oscillation in the brain [34], synthetic genetic oscillators [35], and the dynamics of astrocyte cultures [36]. It has been also used to investigate several aspects of the dynamics of neuronal and FHN coupled models [36–40], as well as Hodgkin–Huxley neurons [41,42].

The issue of the overall external influence on individual elements in ensembles is common to many fields, including neural networks [43]. A common noise can moreover play a constructive role [44]. On the other hand, correlated inputs in interacting neural networks are frequently used to explore pool's dynamics and potential network capabilities, being the visual system the paradigmatic case. For example, failures of binocular integration and visual threshold have been usually investigated by forcing both eyes with conunterphase stimulation at low temporal frequency from a long time ago [45,46]. This scenario has also been expanded to include spatial frequency in the external forcings (in the case of retina). Also, counterphase gratings are a frequently used tool to investigate network dynamics, for example the one associated to binocular vision [47].

Our focus is the study of synchronization processes in populations of interacting nonlinear oscillators. In previous studies [48–52] we have been addressing the noise sustained synchro-

* Corresponding author.
E-mail addresses: sanchez@mdp.edu.ar (A.D. Sánchez), izus@mdp.edu.ar (G.G. Izús).
[1] Member of CONICET, Argentina.

http://dx.doi.org/10.1016/j.physleta.2016.04.017
0375-9601/

nization of rings whose units (displaying excitable FHN dynamics) are coupled in phase-attractive or phase-repulsive way. In all the cases, we found coupling induced nonequilibrium structures called antiphase state (APS), in which the neurons of the ring alternate regularly (except for noise-induced defects) their excitation states in space. In particular, we have made theoretical estimations of the noise thresholds for activation and synchronization of the APS in FHN systems. This analysis was facilitated because nonequilibrium potential (NEP) [53] is known for the system [54,55]. The NEP—a non-equilibrium analog of free energy—provides deep insight on the dynamical mechanisms leading to pattern formation, and other phenomena where fluctuations play a constructive role [2,56].

Here we extend that analysis to explore cooperative effects between phase repulsive and phase attractive synapses in structured networks under non-uniform external forcing. In particular we consider two networks of phase-repulsively linked units, which are externally forced with opposite phases by a subthreshold signal (this configuration is expected to induce noise-sustained synch in counterphase). These networks are in turn phase-attractively linked each other by electrical synapses, in order to allow the interplay of both kinds of coupling. A competition scenario is thus expected between electric coupling and external forcing: whereas coupling tends to keep both networks in phase, external forcing favors a counterphase dynamical state. We present numerical evidence of noise-sustained activation and synchronization, and we show that the resonant dynamics can be explained in terms of noise-sustained transitions between NEP attractors, as they exchange adiabatically their relative stability obeying the slow subthreshold signals. These are the fundamental ingredients driving the dynamics and determining the relevant noise scales.

In Section 2 we briefly review the dynamic equations of the model; in Sec. 3 we provide numerical evidence of noise sustained synchronization, and characterize the constructive role of noise in the process. Then we elucidate the observed dynamics in terms of the NEP of a reduced model in Sec. 4, and collect our conclusions in Sec. 5.

2. The model

The FHN model is one of the most paradigmatic mathematical models in theoretical research on neural networks. It emerges as a two-dimensional simplification of the four-dimensional Hodgkin–Huxley one, in which only the membrane potential and a recovery variable are represented. The FHN model is also an archetypal model of activator–inhibitor systems, and a simple representation of excitable firing dynamics; it is capable of displaying periodic oscillations, stable fixed points, and excitability [57]. The constructive effects of noise on the FHN model have been widely reported in literature in a variety of phenomena [1–3].

In order to analyze the synchronization between networks displaying noise-sustained activities, we consider a minimal block of a structured FHN neuronal network, composed of two identical phase-repulsive coupled rings. One of them (network I) is externally forced by a subthreshold periodic signal while the other (network II) is electrically coupled with the first ring in such a way that its external forcing has an opposite phase than the one applied to network I (see Fig. 1). Inside each network nearest-neighbor antiphase-coupling among activator variables is assumed. This kind of coupling is known to sustain noise-induced activity by a well-established mechanism [49]. Coupling parameters are assumed to be independent of the presynaptic and postsynaptic membrane potentials, and can therefore be modeled by constants D and E, while the coupling between arrays is proportional to the difference of presynaptic and postsynaptic membrane potentials (electrical coupling). The equations for the model are

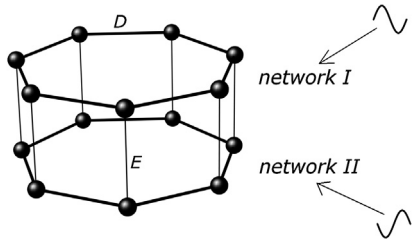

Fig. 1. Schematic graph of the system structure: thin lines denote electrical coupling (E), while thick lines denote antiphase coupling (D). All cells are externally forced and the relative phase of the external signals are indicated.

$$\dot{u}_i = bu_i(1-u_i^2) - v_i + S(t) - D(u_{i+1}+u_{i-1}) + E(p_i-u_i) + r_1\,\xi_i^{(u)}(t) + r_2\,\xi_i^{(v)}(t) \quad (1)$$

$$\dot{v}_i = \epsilon(\beta u_i - v_i + C) + r_3\,\xi_i^{(u)}(t) + r_4\,\xi_i^{(v)}(t) \quad (2)$$

$$\dot{p}_i = bp_i(1-p_i^2) - q_i - S(t) - D(p_{i+1}+p_{i-1}) + E(u_i-p_i) + r_1\,\xi_i^{(p)}(t) + r_2\,\xi_i^{(q)}(t) \quad (3)$$

$$\dot{q}_i = \epsilon(\beta p_i - q_i + C) + r_3\,\xi_i^{(p)}(t) + r_4\,\xi_i^{(q)}(t). \quad (4)$$

The activator (u_i in network I, p_i in network II) is the fast variable, which mimics the action potential off cell i; the inhibitor (v_i in network I, q_i in network II) is the slow—or recovery—variable, which is related to the time dependent conductance of the potassium channels in the membrane [32]. Here $i = 1,\ldots,N$; $u_{N+1} \equiv u_1$, $u_0 \equiv u_N$, $p_{N+1} \equiv p_1$, $p_0 \equiv p_N$. The subthreshold external signal $S = A_0 \sin\omega t$ is injected in both networks with opposite phase. ϵ is the activator–inhibitor timescales ratio, $D > 0$ is the antiphase-coupling strength within each network, while $E > 0$ is the electric coupling strength between networks. Finally, $\xi_i^{(k)}$ are Gaussian white noises with $\langle \xi_i^{(k)}(t)\rangle = 0$ and $\langle \xi_i^{(k)}(t)\,\xi_j^{(m)}(t')\rangle = \eta\,\delta_{i,j}\,\delta_{k,m}\,\delta(t-t')$, where η is the common noise intensity and $k, m \in \{u, v, p, q\}$.

Throughout the work, the following values have been adopted: $N = 256$, $\epsilon = \beta = 10^{-2}$, $b = 3.5\times10^{-2}$, $C = 2\times10^{-2}$, $D = 10^{-2}$, $A_0 = 1.1\times10^{-2}$, $\omega = 2\times10^{-3}$, $\epsilon r_1 = r_3 = \cos 0.05$ and $\epsilon r_2 = r_4 = \sin 0.05$. The values of the parameters are not totally arbitrary: the value of D is selected in order to have a well-developed regime of noise-sustained synchronization in externally forced isolated networks [50], while the period $T = 2\pi/\omega$ remains above the typical deterministic time (i.e. the turnaround time of a single spike), so that the signal can be regarded as an adiabatic perturbation. Besides, single-cell parameters and noise coefficients have been selected in such a way that they satisfy an integrability condition, required by the theoretical characterization of the dynamics [see Eq. (10) in Sec. 4].

3. Noise sustained synchronization

Following [50] we call activated or excited those cells for which the activator field exceeds some threshold value u_{th}. To quantify the level of activity of each network, we introduce the normalized global activity

$$A(t) = \frac{1}{N}\sum_{i=1}^{N} \Theta[x_i(t) - u_{th}]. \quad (5)$$

Here x_i represents either u_i or p_i (depending on the network we refer to), and Θ is the Heaviside step function. As expected, $A(t)$ is not sensitive to u_{th} for reasonable values of threshold. Hereafter we fix $u_{th} = 0.4$. Due to the fact that an excited neuron inhibits its neighbors through the antiphase-coupling, we often observe spatially alternating states of excited and inhibited cells, i.e. APS. Note

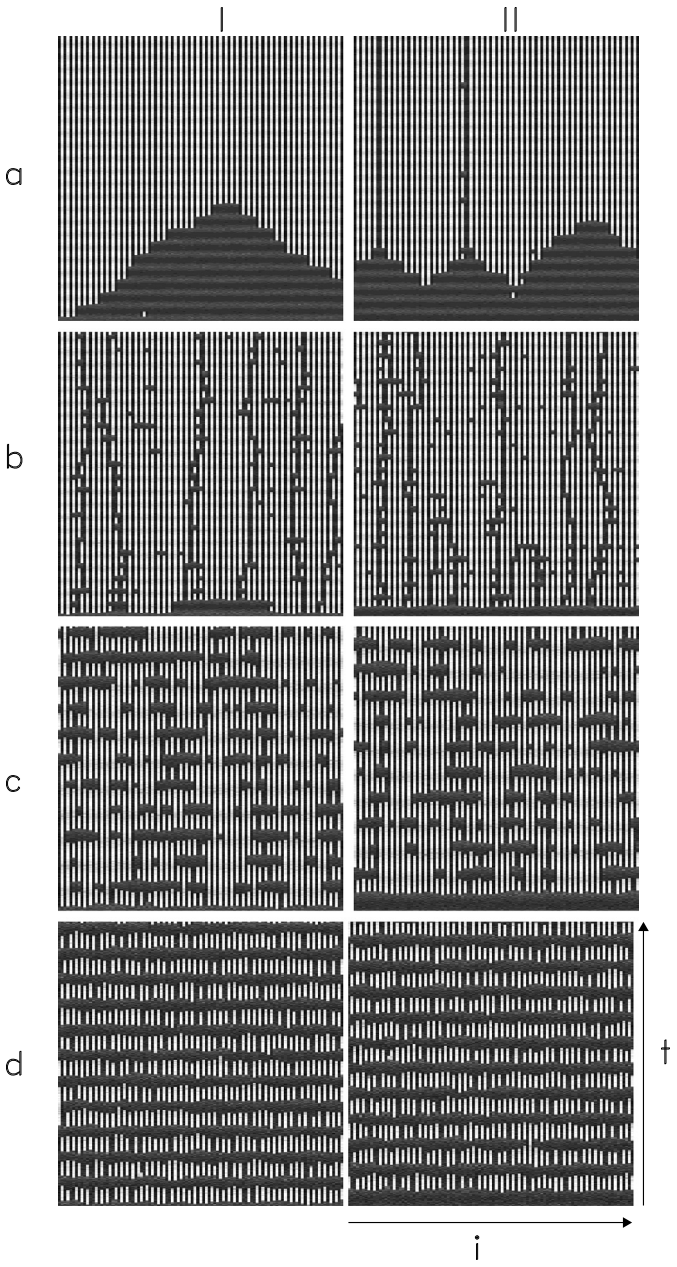

Fig. 2. Activity record of subsets of 100 neurons in network I (left) and in network II (right), with coupling intensity $E = 10^{-4}$. White: activated cells; black: inhibited cells. (a) and (b): 22 periods of the signal, and noise intensities (a) $\eta = 2 \times 10^{-8}$, (b) 5×10^{-8}; (c) and (d) 11 periods of the signal, and noise intensities (c) 10^{-7} and (d) 2.2×10^{-7}.

that a perfect APS would correspond to $A = 1/2$. However, A does not reach, in general, this value because alternance fails due to the local noises.

An indicator of the synchrony of each network with the external signal $S(t)$ is the Q-factor, defined by

$$Q = \sqrt{Q_{\sin}^2 + Q_{\cos}^2}, \quad \text{with} \tag{6}$$

$$Q_{\sin} = \frac{1}{nT} \int_0^{nT} 2A(t) \sin(\omega t) dt$$

$$Q_{\cos} = \frac{1}{nT} \int_0^{nT} 2A(t) \cos(\omega t) dt,$$

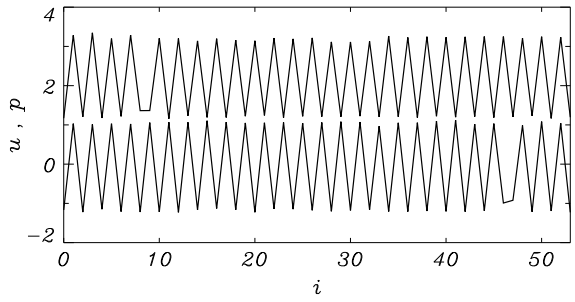

Fig. 3. Snapshot of corresponding segments of the networks for $E = 10^{-4}$ and $\eta = 2 \times 10^{-8}$ (as in Fig. 2a). For the sake of clarity, the p field is shifted upwards by two units. We show a full domain in counterphase configuration limited by in-phase state configurations. We remark that for these particular values of the parameters, both networks are mainly in phase.

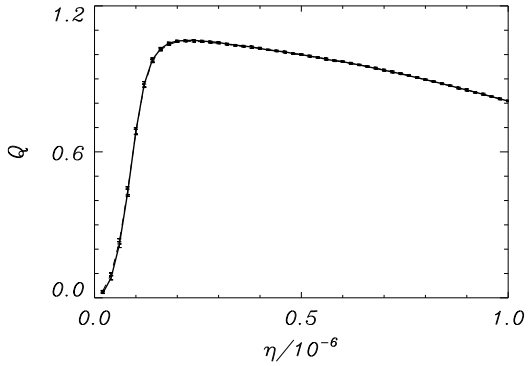

Fig. 4. Q-factor for network I at $E = 10^{-4}$. The Q-Factor for network II almost coincides with this, and cannot be distinguished in the graph.

where n is the number of periods T covered by the integration time.

A global view of the dynamics is provided by Fig. 2, which compares the activity records of equivalent subsets of neurons in each ring, for $E = 10^{-4}$ and different noise intensities.

For weak noise (case not shown) there are only subthreshold oscillations, due to the signal. By increasing the noise intensity and after a transient, both networks become activated (as shown in Fig. 2a, where both systems are in APS). Due to the presence of defects, corresponding segments in both networks can be either in phase or in counterphase, as illustrated in Fig. 3. Numerical simulations show that in-phase activation is more frequent than counterphase one, and the asymmetry increases with the coupling strength (not shown). Increasing the noise level further (Fig. 2b) a larger number of defects arise, and for a suitable noise level the networks synchronize with the forcing (Figs. 2c and 2d). As the injected signals are in counterphase, we see that whilst one network remains in the APS, the other one is in the uniform state. The synchronization degrades for still larger noise level, as shown in Fig. 4, where the Q-factor is plotted vs noise intensity. The maximum synchronization occurs for $\eta \approx 2.2 \times 10^{-7}$.

4. Theoretical description of the dynamics via the NEP

4.1. Nonequilibrium potential

The nonequilibrium potential (NEP) Φ for Langevin-type equations has been defined [53] as the zero-noise limit of the logarithm of the stationary probability density function

$$P^{\text{stat}}(\mathbf{W}, \eta) = Z(\mathbf{W}) \exp\left[-\frac{\Phi(\mathbf{W})}{\eta} + \mathcal{O}(\eta)\right], \tag{7}$$

where the variables of the problem have been grouped in a vector **W**. The NEP is a Lyapunov function of the deterministic dynamics and provides information on the properties of attractors. In particular, it determines the height of the barriers separating attraction basins, which in turn define the transition rates among the different attractors. Another way to define a NEP, which remains valid even outside the small noise limit was proposed by Ao [58].

The NEP for a general network of linearly coupled FitzHugh–Nagumo cells has been derived in [50]. Since the two networks defined in our model determine in turn a single network with a particular coupling structure, we can apply the results of [50] to the present case. We obtain

$$\Phi = \sum_{i=1}^{N}\left[\Phi_s(u_i,v_i)+\Phi_s(p_i,q_i)-\frac{2}{\lambda_1}S(t)(u_i-p_i)+\frac{2D}{\lambda_1}(u_iu_{i+1}+p_ip_{i+1})+\frac{E}{\lambda_1}(u_i-p_i)^2\right], \tag{8}$$

$$Z = \text{constant}, \tag{9}$$

Φ_s being the NEP for a single cell without signal, given by

$$\Phi_s(u,v)=\frac{\epsilon}{\lambda_2}(v^2-2\beta uv-2Cv)+\frac{2\lambda\epsilon}{\lambda_1\lambda_2}(\beta u^2+2Cu)-\frac{2}{\lambda_1}\left[\frac{b}{2}u^2-\frac{b}{4}u^4\right],$$

where $\lambda_1 = r_1^2+r_2^2$, $\lambda_2 = r_3^2+r_4^2$ and $\lambda = r_1r_3+r_2r_4$. Integrability conditions—arising from the NEP's derivation—constrain the parameters to obey

$$\beta\lambda_1+\lambda_2/\epsilon = 2\lambda. \tag{10}$$

The third term in Eq. (8) is the explicit contribution of the signal, the fourth one takes into account the antiphase-coupling inside each network and the last one, the electrical coupling between both rings.

4.2. Reduced four-neuron model

A theoretical study of the dynamics can be done by exploiting the properties of the NEP during time-evolution. To this end we consider a simplified model, where each network is represented by a two-neuron system: a minimal description of an idealized case where all the even nodes on one hand, and all the odd nodes on the other, have the same stochastic phase-space trajectory. For this four-neuron model, the NEP in Eq. (8) takes the form:

$$\Phi(u_1,v_1,\ldots,p_2,q_2)=\Phi_s(u_1,v_1)+\Phi_s(u_2,v_2)+\Phi_s(p_1,q_1)+\Phi_s(p_2,q_2)-\frac{2}{\lambda_1}S(u_1-p_1+u_2-p_2)+\frac{4D}{\lambda_1}(u_1u_2+p_1p_2)+\frac{E}{\lambda_1}[(u_1-p_1)^2+(u_2-p_2)^2]. \tag{11}$$

The critical points (minima and saddles) of the NEP are the fixed points of the dynamics, and can be alternatively determined by the intersection of the nullclines. Although Eqs. (1)–(4) are not gradient, the nonvariational contribution to the dynamics also vanishes at the fixed points due to the particular structure of the probability current [50].

As far as we are interested only in barrier heights—given by the NEP difference $\Delta\Phi$ between saddle points and minima—we project out the NEP along the slow manifolds $v_{1,2} = \beta u_{1,2} + C$, $q_{1,2} = \beta p_{1,2} + C$ of Eqs. (1)–(4), which capture all the system's fixed points. We thus concentrate on $\Phi(u_1,u_2,p_1,p_2)$ and proceed to characterize their minima and saddles.

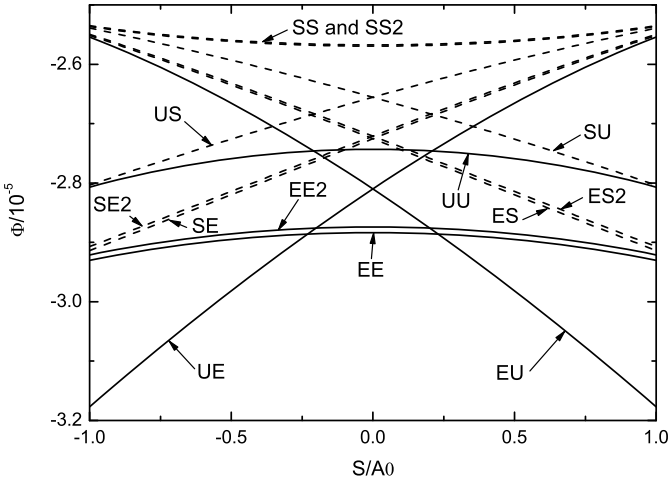

Fig. 5. NEP values at the minima (solid lines) and saddles (dashed lines) of the four-neuron model, for $E = 10^{-4}$. State SS has lower NEP value than SS2, but the small difference cannot be appreciated in the figure.

In the following, U, E and S will respectively denote the uniform state, APS and saddle fixed points in each network of the reduced model [59]. U is characterized by $u_1 \approx u_2 \approx -1$ in network I or $p_1 \approx p_2 \approx -1$ in network II, and corresponds to the uniform state in the real network. In E, one neuron becomes excited and the other one remains inhibited (either $u_1 \approx -u_2 \approx 1$ or $-u_1 \approx u_2 \approx 1$ in network I, or correspondingly in network II), which corresponds to an APS in the real network. Finally S is an intermediate state (e.g. $u_1 \approx -1$ and $u_2 \approx 0$ in network I), which corresponds to a high-dimensional saddle point lying between the rest state and APS in the real network.

This done, we introduce a two-letter code to label the fixed points of the reduced model [59] (the first letter corresponds to network I, and the second one to network II). Accordingly, UU denotes the state where both networks are in the uniform state, and EE the one where both networks are in the APS. Now, whereas UU is unique, the remaining states are doubly degenerate under simultaneous permutations of u_1 by u_2 and p_1 by p_2. In one instance of some states, the inhibited neurons in each network are electrically coupled; in the other, they are not. We distinguish those cases by adding a two in the code for the second case (e.g. we label as SE2 the state where $u_1 \approx -p_1 \approx p_2 \approx -1$ and $u_2 \approx 0$). It is worth noting that if at least one letter in the code is S, the whole state corresponds to a saddle point in the NEP (that is why the single-network intermediate state is labeled as S).

4.3. Activation chains

As we will show, the dynamics can be interpreted mainly as a succession of noise-activated transitions between metastable attractors. The process to escape from a given minimum through a barrier is an activation process, where the energy for the jump comes from the noise. The order of magnitude of noise intensity to escape can be obtained as (see Appendix A)

$$\eta \approx \frac{\Delta\Phi}{4}. \tag{12}$$

To elucidate the dynamics, we consider how the NEP at the attractors and repellers involved in the route to synchronization behave with the signal. As in the simulations, the system is assumed to start always in the UU uniform state.

The NEP landscape depends on the electric coupling strength. For low enough values ($E \leq 6\times10^{-4}$), the reduced model has the structure of barriers shown in Fig. 5 for $E = 10^{-4}$. For low

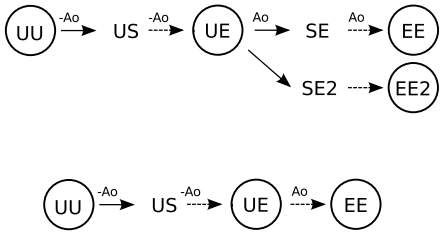

Fig. 6. Schemes of activation transition chains. The upper frame corresponds to $E \leq 6 \times 10^{-4}$, and the lower one to $7 \times 10^{-4} \leq E \leq 1.3 \times 10^{-2}$. Solid arrow: noise-induced transition; dashed arrow: deterministic transition; circles: metastable states. The $\pm A_0$ over arrow indicate at which (approximate) signal value the transition take place. The deterministic (not saddle-mediated) transition from UE to EE is due to the collapse of UE state at $S \approx A_0$.

noise intensities the system remains in UU, performing subthreshold oscillations. A noise level of $\eta_A \approx 8.8 \times 10^{-9}$ allows to reach UE (across US) at $S = -A_0$. Once in UE, for this level of noise, the system jumps to EE at $S = A_0$ (through the SE saddle, with a barrier $\eta_B \approx 6.4 \times 10^{-9}$). η_A is the threshold for activation, because once in EE, the system cannot escape from it. Increasing noise intensity to $\eta_C \approx 10^{-8}$, another transition (to EE2, through SE2) becomes possible. A sketch of transition chains and branches for low E values is shown in the upper frame of Fig. 6. Note that since $\eta_B < \eta_C$, the upper branch (ending in EE, i.e. in-phase activated networks) is more probable than the lower one (ending in EE2, i.e. counterphase activated networks). Examples of both states of the model can be seen as domains in the real system (Fig. 3).

To advance in the synchronization cycle it is necessary to exit from EE, or eventually from EE2 (as in the upper frame of Fig. 7). In the first case, reaching EU (across ES) at $S = A_0$ requires a noise level $\eta_s = \Delta\Phi/4 \approx 4.1 \times 10^{-8}$. In the second, the transition EE2 $\rightarrow$ ES2 $\rightarrow$ EU at $S = A_0$ has a smaller barrier $\eta_{s'} = \Delta\Phi/4 \approx 3.6 \times 10^{-8}$. However, the second route requires having reached EE2, a less probable event as already stated. In conclusion, with noise intensity η_s the system goes from UE to EU either through EE or through EE2. To close the synchronization cycle, the system follows the route EU $\rightarrow$ ES (ES2) $\rightarrow$ EE (EE2) $\rightarrow$ SE (SE2) $\rightarrow$ UE. This route does not introduce any new threshold. As a consequence, η_s is the predicted threshold for synchronization.

Due to the symmetry of the system, (a) the states with two repeated letters (UU, EE, EE2, SS, and SS2) are even functions of the instantaneous value of the signal, and (b) the states with two different letters have a "reflected" state with the same NEP (e.g. US and SU) when changing S to $-S$. For that reason, each transition described has its counterpart—with the same value of activation but with the sign of the signal changed—and the transition takes place between states labeled with exchanged letters. For example, although we only mentioned UU $\rightarrow$ US $\rightarrow$ EU at $S = -A_0$, we also have UU $\rightarrow$ SU $\rightarrow$ UE at $S = A_0$.

In some cases, the barriers at $S = \pm A_0$ decrease as E increases, and can even disappear through saddle-node collapse. Nevertheless the states remain for smaller values of the signal. Due to the dimensionality of the reduced model, it is not straightforward to represent the NEP landscape. A useful indicator is the number of critical points for each E interval, as summarized in Table 1. If n is the number of critical points found in the table for a given E, then the total number of critical points is $2n-1$, because UU is the only one not degenerated (and it exists for any signal and E values). The numbers between parentheses count the critical points that are metastable states of the system, i.e. minima of the NEP. Note that due to the symmetry of the system (reflected in the symmetry of the curves in Fig. 5), when a state labeled with two repeated letters disappears for $S = 0$, it disappears for all values of S. The last column on the table indicates the critical points in the immediately upper row that had disappeared. Critical points in bold characters disappear at $S = 0$, otherwise, they disappear at $S = A_0$.

Table 1
Number of critical points (and of minima, between parentheses), not counting degeneration, of the NEP for each interval of the electrical coupling E between networks.

E interval	# crit. p. $S = 0$	# crit. p. $S = \pm A_0$	disappear at $S = A_0$ and at $S = 0$ (bold)
$[0, 6 \times 10^{-4}]$	13 (5)	13 (5)	–
$[7 \times 10^{-4}, 8 \times 10^{-4}]$	13 (5)	11 (4)	UE, SE
$[9 \times 10^{-4}, 1.3 \times 10^{-3}]$	13 (5)	9 (4)	US, SS
$[1.4 \times 10^{-3}, 1.7 \times 10^{-3}]$	13 (5)	7 (3)	EE2, ES2
$[1.8 \times 10^{-3}, 6.1 \times 10^{-3}]$	13 (5)	5 (3)	SE2, SS2
$[6.2 \times 10^{-3}, 6.4 \times 10^{-3}]$	9 (3)	5 (3)	**EU, ES, UE, SE**
$[6.5 \times 10^{-3}, 1.3 \times 10^{-2}]$	5 (2)	5 (3)	**EE2, SE2, ES2, SS2**
$[1.4 \times 10^{-2}, \infty)$	3 (2)	3 (2)	**US, SU**, EU, ES

Next, we analyze the predictions (of the four-neuron model), for activation processes for larger values of E. We showed that for small enough coupling (upper frame in Fig. 6) the threshold for in-phase activation is determined by the barrier UU $\rightarrow$ US (at $S = -A_0$) in the chain UU $\rightarrow$ US $\rightarrow$ UE $\rightarrow$ SE $\rightarrow$ EE. On the other hand, the threshold for counterphase activation is determined by the barrier UE $\rightarrow$ SE2 (at $S = A_0$) in the chain UU $\rightarrow$ US $\rightarrow$ UE $\rightarrow$ SE2 $\rightarrow$ EE2. Fig. 8 summarizes a NEP analysis performed including the coexistence regime of in-phase and counterphase states, where all the barriers that organize the dynamics are included. Once occupied state UE, the barrier represented by SE2 (counterphase activation barrier) grows with E while the alternative barrier (to overcome in order to reach SE) decreases. As a consequence, the in-phase chain becomes more probable than the counterphase one. Eventually, UE disappears at $S = A_0$ (Table 1) and then the UE $\rightarrow$ EE transition becomes deterministic (and the counterphase activation virtually impossible), as schematized in the lower frame of Fig. 6. This mechanism holds for $7 \times 10^{-4} \leq E \leq 1.3 \times 10^{-2}$.

4.4. Synchronization regimes

For E small enough we saw that the evolution from the rest state UU starts with the transition UU $\rightarrow$ US $\rightarrow$ UE. Once in UE, the periodic evolution is given by the following chain of transitions UE $\rightarrow$ SE (SE2) $\rightarrow$ EE (EE2) $\rightarrow$ ES (ES2) $\rightarrow$ EU $\rightarrow$ ES (ES2) $\rightarrow$ EE (EE2) $\rightarrow$ SE (SE2) $\rightarrow$ UE, so closing the cycle (Fig. 7, upper frame). Since for S positive enough, EU has a smaller NEP value than EE and EE2, the transition through either route toward EU proceeds in two steps. The system remains a short time in either EE or EE2 before ending up in EU. The same occurs with the symmetric states at $S = -A_0$. As discussed when describing activation, the chain UE $\rightarrow$ SE $\rightarrow$ EE becomes deterministic for $7 \times 10^{-4} \leq E \leq 1.3 \times 10^{-2}$, simplifying the transition to the decay UE $\rightarrow$ EE. The new scheme is shown in the lower frame of Fig. 7. The highest barrier—which therefore determines the synchronization threshold—is given in both regimes by $\Phi(\text{ES}) - \Phi(\text{EE})$ at $S = A_0$. Fig. 8 shows the dependence on E of the synchronization barrier, which agrees with numerical results for the maxima of Q-factors.

Finally for $E \geq 1.4 \times 10^{-2}$, only three critical points exist (Table 1). To exemplify the dynamics in such situation we consider the strong-coupling limit. For $E \rightarrow \infty$ we have $u_1 = p_1$ and $u_2 = p_2$ in the reduced model, and its NEP reads

$$\Phi(u_1, v_1, u_2, v_2) = 2\left[\Phi_s(u_1, v_1) + \Phi_s(u_2, v_2) + \frac{4D}{\lambda_1}(u_1 u_2)\right]. \tag{13}$$

The dependence on E naturally disappears in this limit, but also the dependence on S. As both networks are perfectly coupled,

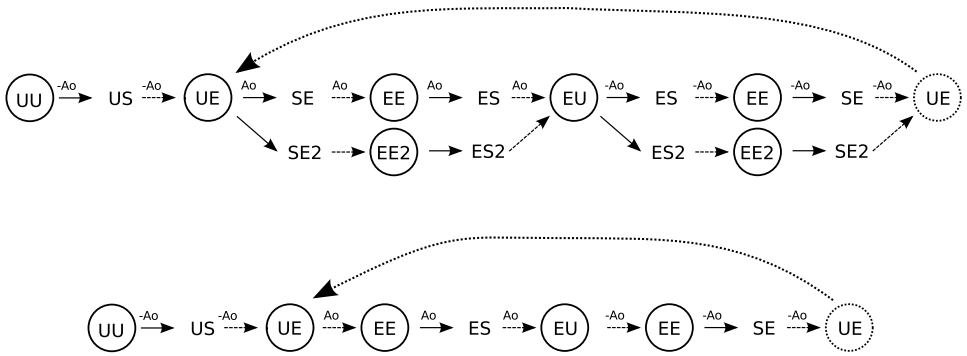

Fig. 7. Schemes of synchronization transition chains. Upper one corresponds to $E \leq 6 \times 10^{-4}$, lower one to $7 \times 10^{-4} \leq E \leq 1.3 \times 10^{-2}$. The UE state in dotted circles is the one at the beginning of the cycle.

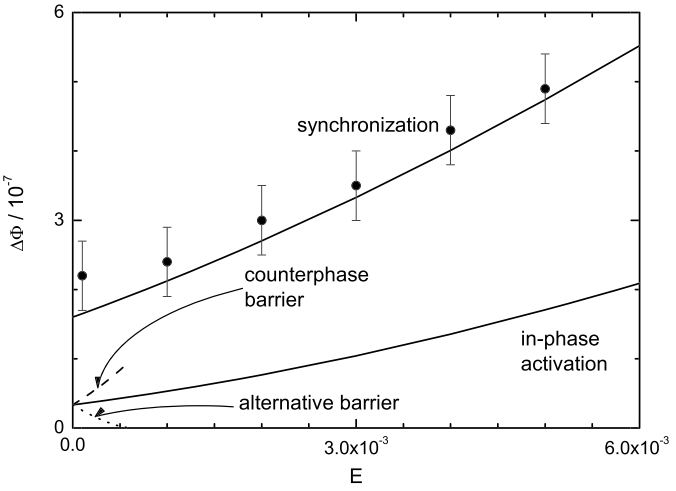

Fig. 8. Relevant barrier heights as functions of the coupling strength E between networks, for in-phase activation $[\Phi(\mathrm{US}) - \Phi(\mathrm{UU})$ at $S = -A_0]$, synchronization $[\Phi(\mathrm{ES}) - \Phi(\mathrm{EE})$ at $S = A_0]$, counterphase $[\Phi(\mathrm{SE2}) - \Phi(\mathrm{UE})$ at $S = A_0]$ and alternative barrier $[\Phi(\mathrm{SE}) - \Phi(\mathrm{UE})$ at $S = A_0]$. Points corresponds to the maxima of Q-factor as result of numerical simulations (average over 10 realizations).

there are only three states (UU, EE, and SS). For that reason, the NEP in these states takes for any E the same value as in the absence of signal, as can be seen by comparing Eqs. (11) and (13). The NEP analysis also shows that a level noise of $[\Phi(\mathrm{SS}) - \Phi(\mathrm{UU})]/4 = 4.3 \times 10^{-7}$ is necessary to escape from UU, and this noise intensity is not enough to escape from EE, i.e. it is the activation threshold. To exit from EE it is necessary to increase the noise up to $[\Phi(\mathrm{SS}) - \Phi(\mathrm{EE})]/4 = 7.8 \times 10^{-7}$, hence no synchronization with the signal is expected. Numerical simulations (not shown) confirm these predictions.

5. Conclusions

We have studied numerically (and analytically within a reduced model) the stochastic dynamics of a system made of excitable FitzHugh–Nagumo neurons, submitted to independent additive Gaussian white noises (with the same intensity η) in each field. They are assembled into two identical rings of phase-repulsively coupled (and thus able to develop noise-sustained structures) which are in turn sitewise electrically coupled, and submitted to opposed but otherwise identical subthreshold harmonic signals. Interplay between phase-attractive and phase-repulsive couplings is then generated by the particular wiring.

Numerical integration shows that in each ring, local additive noises sustain extended anti-phase states (APS), where the cells alternate their activation state along the network: "activated–inhibited–activated–inhibited ...". These APS appear as domains in each ring. Correlations are observed between networks: electrically coupled domains remain mainly in phase, although some of them can be in counterphase. A threshold noise intensity is necessary for the activation, namely for the described structures to appear and remain in time.

For large enough noise intensities, coherent time behavior is observed where both networks exhibit essentially the same synchronized activity—basically a periodic transition in each network between the APS and the uniform rest state—in synchrony with the external forcing but keeping the counterphase relation induced by the signal. Moreover, the Q-factors exhibit maxima as function of η, i.e. there is optimal noise intensity for maximal coherence.

The numerical results can be interpreted by considering the nonequilibrium potential (NEP) of a four-cell reduced model. Analyzing the dependence of the NEP landscape on the external signal, we have shown that the system dynamics can be explained in terms of noise-sustained transitions (and eventually deterministic decays) between attractors—i.e. NEP minima—in such a way that a chain of transitions explains the activation and the synchronization of the system. The noise intensities required for activation and synchronization are quantitatively determined by the highest barrier height in the chain, corresponding to the highest NEP's saddle point. The numerically observed formation of in-phase and counterphase configurations involving extended antiphase states of both networks is theoretically explained in terms of the chains of (mainly) noise-sustained transitions, that originate the structures and their particular correlations. Complete in-phase–counterphase symmetry is predicted and observed only for uncoupled networks, whereas counterphase configurations diminish with coupling intensity E as a reflection of the system's fixed-point structures and their NEP levels. Although naturally, the four-cell model does not take into account the formation of defects, it helps elucidating the route to synchronization, identifying the relative stability of the relevant states and estimating the optimal noise intensity for activation and synchronization.

In addition, we study the dynamics as a function of network coupling. Typically, for small enough noise intensity we have subthreshold adiabatic oscillations, and as the noise intensity grows there is activation and further synchronization. For large coupling ($E \geq 1.4 \times 10^{-2}$) however, synchronization is no longer possible. Levels of activation and synchronization were predicted as functions of E within the four-cell model, and verified by numerical simulations.

Since barrier heights depend on the signal amplitude A_0, all the reported results do. As a rule, η thresholds decrease as A_0 increases. Moreover, increasing A_0 originates attractor collapse (at the extremal values of the signal) much as shown in Table 1 for constant A_0 and increasing E.

As it occurs in related phenomena (e.g. coherence resonance in coupled FitzHugh–Nagumo systems [8]), our results are expected to depend on both temporal and spatial noise correlations. The NEP approach would be useful even in those cases, since dynamics driven by space-correlated or colored (Ornstein–Uhlenbeck) noises can in principle be described in terms of a suitable NEP [33].

Acknowledgements

We thanks R.R. Deza for a critical reading of the manuscript and A. Alés for help with figures. We also acknowledge financial support from CONICET (project PIP 220100100315) and Universidad Nacional de Mar del Plata (project 15/E639), of Argentina.

Appendix A. Noise intensity to escape from a state

Let us call α the departure state, place the origin in α and take $\Phi = 0$ in this state. An expansion of Φ to second order in the NEP's variables $\mathbf{X}$ yields

$$\Phi(\mathbf{X}) = \mathbf{X}^T A\, \mathbf{X}, \tag{A.1}$$

with $\mathbf{X}^T = (x_1, x_2, \ldots, x_n)$ a row vector and A the Hessian matrix $A_{ij} = \partial^2\Phi/(\partial_{x_i}\partial_{x_j})$ evaluated at state α. By the NEP's definition [Eq. (7)], we can approximate the stationary joint probability density function for $\mathbf{X}$ when the system is in state α by

$$P(\mathbf{X}) = \frac{\sqrt{\det A}}{\pi^{n/2}} \exp\left(-\frac{\mathbf{X}^T A\, \mathbf{X}}{\eta}\right). \tag{A.2}$$

Hence the NEP's mean is $\langle\Phi\rangle = n\,\eta/2$. We adopt the criterion $\Phi_{\text{sad}} = \langle\Phi\rangle$ and then the estimated noise intensities for the transition—having into account that $\Phi_{\text{sad}} = (N/2)\Delta\Phi$ and $n = 4N$ (each neuron has two variables)—is

$$\eta = \frac{\Phi_{\text{sad}}}{4}. \tag{A.3}$$

This equation determine η as an intensive parameter, and then improves the cruder approximation in Ref. [59] (obtained from equating the height barrier Φ_{sad} to the NEP standard deviation).

References

[1] J. García-Ojalvo, J.M. Sancho, Noise in Spatially Extended Systems, Springer, New York, 1999.
[2] F. Sagués, J.M. Sancho, J. García-Ojalvo, Rev. Mod. Phys. 79 (2007) 829.
[3] R. Toral, C.J. Tessone, J. Viana Lopes, Eur. Phys. J. Spec. Top. 143 (2007) 59.
[4] L. Gammaitoni, P. Hänggi, P. Jung, F. Marchesoni, Rev. Mod. Phys. 70 (1998) 223.
[5] K. Wiesenfeld, F.J. Jaramillo, Chaos 8 (1998) 539.
[6] T. Wellens, V. Shatokhin, A. Buchleitner, Rep. Prog. Phys. 67 (2004) 45.
[7] H.S. Wio, Phys. Rev. E 54 (1996) R3075.
[8] A.S. Pikovsky, J. Kurths, Phys. Rev. Lett. 78 (1997) 775.
[9] C. Zhou, J. Kurths, Phys. Rev. Lett. 88 (2002) 230602.
[10] C.J. Tessone, A. Sciré, R. Toral, P. Colet, Phys. Rev. E 75 (2007) 016203.
[11] A. Pikovsky, M. Rosenblum, J. Kurths, Synchronization: A Universal Concept in Nonlinear Sciences, Cambridge, UK, 2003.
[12] J.A.K. Suykens, G.V. Osipov, Chaos 18 (2008) 037101.
[13] T. Nowotny, R. Huerta, M.I. Rabinovich, Chaos 18 (2008) 037119.
[14] C.M. Gray, W. Singer, Proc. Natl. Acad. Sci. USA 86 (1989) 1698.
[15] M. Bazhenov, M. Stopfer, M. Rabinovich, R. Huerta, H.D.I. Abarbanel, et al., Neuron 30 (2001) 553.
[16] M.R. Mehta, A.K. Lee, M.A. Wilson, Nature 417 (2002) 741.
[17] D.S. Lee, Phys. Rev. E 72 (2005) 026208.
[18] A.E. Motter, C.S. Zhou, J. Kurths, Europhys. Lett. 69 (2005) 334.
[19] C. Zhou, J. Kurths, Phys. Rev. Lett. 96 (2006) 164102.
[20] A. Arenas, A. Diaz-Guilera, C.J. Perez-Vicente, Physica D 224 (2006) 27.
[21] Q.Y. Wang, Q.S. Lu, G.R. Chen, D.H. Guo, Phys. Lett. A 356 (2006) 17.
[22] T. Kunichika, Y. Tetsuya, A. Kazuyuki, K. Hiroshi, Int. J. Bifurc. Chaos 13 (2003) 653.
[23] I. Belykh, E. de Lange, M. Hasler, Phys. Rev. Lett. 94 (2005) 188101.
[24] M. Oh, V. Matveev, J. Comput. Neurosci. 26 (2009) 303.
[25] S. Achuthan, C.C. Canavier, J. Neurosci. 29 (2009) 5218.
[26] K. Kitajo, S.M. Doesburg, K. Yamanaka, D. Nozaki, L.M. Ward, et al., Europhys. Lett. 80 (2007) 40009.
[27] A. Neiman, L. Schimansky-Geier, A. Cornell-Bell, F. Moss, Phys. Rev. Lett. 83 (1999) 4896.
[28] E. Yilmaz, M. Uzuntarla, M. Ozer, M. Perc, Physica A 392 (2013) 5735.
[29] E. Yilmaz, Chaos Solitons Fractals 66 (2014) 1.
[30] M. Uzuntarla, E. Yilmaz, A. Wagemakers, M. Ozer, Commun. Nonlinear Sci. Numer. Simul. 22 (2015) 367.
[31] G.V. Osipov, J. Kurths, C. Zhou, Synchronization in Oscillatory Networks, Springer, Berlin, 2007.
[32] N.B. Janson, A. Balanov, E. Schöll, Phys. Rev. Lett. 93 (2004) 010601.
[33] A. Schenzle, T. Tél, Phys. Rev. A 32 (1985) 596.
[34] L. Yan, N.C. Foley, J.M. Bobula, L.J. Kriegsfeld, R. Silver, J. Neurosci. 25 (2005) 9017.
[35] E. Ullner, A. Zaikin, E.I. Volkov, J. García-Ojalvo, Phys. Rev. Lett. 99 (2007) 148103.
[36] G. Balázsi, A. Cornell-Bell, A.B. Neiman, F. Moss, Phys. Rev. E 64 (2001) 041912.
[37] E.I. Volkov, E. Ullner, J. Kurths, Chaos 15 (2005) 023105.
[38] C.J. Tessone, E. Ullner, A.A. Zaikin, J. Kurths, R. Toral, Phys. Rev. E 74 (2006) 046220.
[39] A. Sherman, J. Rinzel, Proc. Natl. Acad. Sci. USA 89 (1992) 2471.
[40] Q. Zhao, C.G. Yao, M. Yi, Eur. Phys. J. B 84 (2011) 299.
[41] Y. Li, G. Schmid, P. Hänggi, L. Schimansky-Geier, Phys. Rev. E 82 (2010) 061907.
[42] X. Ao, P. Hänggi, G. Schmid, Math. Biosci. 245 (2013) 49.
[43] Y. Yoshimura, J. Dantzker, E. Callaway, Nature 433 (2005) 868.
[44] D.S. Goldobin, A.S. Pikovsky, Phys. Rev. E 71 (2005) 045201(R).
[45] F. Ireland, J. Exp. Psychol. 40 (1950) 282.
[46] C. Baker, Percept. Psychophys. 8 (1970) 406.
[47] D.M. Levi, A.F. Pass, R.E. Manny, Br. J. Ophthalmol. 66 (1982) 57.
[48] G.G. Izús, R.R. Deza, A.D. Sánchez, AIP Conf. Proc. 887 (2007) 89.
[49] G.G. Izús, A.D. Sánchez, R.R. Deza, Physica A 388 (2009) 967.
[50] A.D. Sánchez, G. Izús, Physica A 389 (2010) 1931.
[51] M.G. dell'Erba, G. Cascallares, A.D. Sánchez, G. Izús, Eur. Phys. J. B 87 (2014) 82.
[52] A.D. Sánchez, G.G. Izús, M.G. dell'Erba, R.R. Deza, Phys. Lett. A 378 (2014) 1579.
[53] R. Graham, in: E. Tirapegui, D. Villarroel (Eds.), Instabilities and Nonequilibrium Structures, D. Reidel, Dordrecht, 1987, pp. 271–290.
[54] G.G. Izús, R.R. Deza, H.S. Wio, Phys. Rev. E 58 (1998) 93.
[55] G.G. Izús, R.R. Deza, H.S. Wio, Comput. Phys. Commun. 121 (1999) 406.
[56] H.S. Wio, R.R. Deza, Eur. Phys. J. Spec. Top. 146 (2007) 111.
[57] J.A. Acebrón, A.R. Bulsara, W.J. Rappel, Phys. Rev. E 69 (2004) 026202.
[58] P. Ao, J. Phys. A, Math. Gen. 37 (2004) L25.
[59] G. Cascallares, A.D. Sánchez, M.G. dell'Erba, G.G. Izús, Physica A 433 (2015) 356.